Letter

Efficient control of high harmonic terahertz generation in carbon nanotubes using the Aharonov-Bohm effect

Yuta Murakami,[1] Kohei Nagai,[2] and Akihisa Koga[2]
[1]*Center for Emergent Matter Science, RIKEN, Wako, Saitama 351-0198, Japan*
[2]*Department of Physics, Tokyo Institute of Technology, Meguro, Tokyo 152-8551, Japan*

(Received 9 March 2023; revised 19 June 2023; accepted 20 November 2023; published 7 December 2023)

We show that high harmonic generation (HHG) in carbon nanotubes (CNTs) can be efficiently controlled using the Aharonov-Bohm (AB) effect. When a static magnetic field (B) is applied along the tube, electronic wave functions acquire complex phases along the circumferential direction (the AB effect), which modifies the band structure. When the magnetic field is applied to metallic CNTs, which can be regarded as one-dimensional massless Dirac systems, realistic values of B lead to a nonzero gap in the THz regime. We demonstrate that such a change from gapless to gapped Dirac systems drastically increases the HHG intensity in the THz regime. In the gapless Dirac system, the velocity of each electron never changes under the electric field, and thus there is no HHG. On the other hand, the gap opening activates both the interband and intraband currents, which strongly contribute to HHG. Our work demonstrates a unique way to manipulate HHG in nanotubes by tuning electronic wave functions using the magnetic field and the tube structure.

DOI: 10.1103/PhysRevB.108.L241202

The recent development of strong lasers in the terahertz (THz) and midinfrared regimes enables us to study various nonlinear and nonequilibrium phenomena in condensed matter [1–7]. Among them, high harmonic generation (HHG), where the higher harmonics of the laser injected into materials are radiated, is a fundamental and technologically important example [8–10]. HHG was originally studied in gas systems [11–13]. Recently, HHG in condensed matter has been observed, and the scope of the HHG research is widely extended to conventional semiconductors, band insulators [14–28], topological materials [29–36], and strongly correlated systems [37–50].

Condensed matter is considered an interesting playground for HHG research for at least two good reasons. First, the periodic potential from atoms, which is absent in gaseous systems, can lead to the peculiar motion of electrons under a strong electric field. An interesting example is the Dirac system, which is characterized by nonparabolic band dispersion. Due to the nonlinear dynamics of electrons in the vicinity of the Dirac node, such systems are theoretically expected to exhibit large nonlinearity [51–60]. HHG was experimentally studied for two-dimensional (2D) Dirac systems realized in graphene [30,31] and on the surface of topological insulators [29,35,36], and for the 3D Dirac system in Cd_3As_2 [34,61]. It was reported that the efficiency of HHG is indeed large compared to other systems [31,34,35], although the origin of HHG is not necessarily the theoretically expected process [31,62]. The second reason is the controllability of HHG. Generally, the properties of condensed matter can be tuned by system parameters such as temperature and doping level, which can be also applicable to HHG. For example, a peculiar HHG dependence on crystal orientations [14,26], electronic phases [37,44,45,47,48], physical pressure [63], and doping [49,64,65] has been proposed theoretically or been observed experimentally.

In this Letter, we propose a unique way to efficiently control HHG in carbon nanotubes (CNTs) combining the physics of the Dirac system and the Aharonov-Bohm (AB) effect [see Fig. 1(a)]. The proposed setup provides an ideal platform to study HHG in Dirac systems, systematically. When the static magnetic field (B) is applied along the tube, electrons in the CNT gain complex phases along the circumferential direction, which modifies the band structure (the AB effect) [66–69]. In particular, metallic CNTs, which can be regarded as 1D massless Dirac systems, become massive Dirac systems when $B \neq 0$. This change qualitatively modifies the electron dynamics, and drastically enhances HHG.

In the dipolar gauge [70–72], the tight-binding Hamiltonian for the CNT with a magnetic field and ac electric field $[E(t)]$ along the tube is expressed as

$$\hat{H}(t) = -t_{\rm hop} \sum_{\langle ij \rangle} e^{i\frac{q}{\hbar}\boldsymbol{A}(t)\cdot\mathbf{r}_{ij}} \hat{c}_i^\dagger \hat{c}_j - \mu \sum_i \hat{n}_i. \tag{1}$$

$\hat{c}_i^\dagger$ is the creation operator of an electron at the ith site and we neglect the spin degrees of freedom. $\langle ij \rangle$ indicates the nearest-neighbor sites, $t_{\rm hop}$ is the hopping parameter, q is the charge of an electron, $\hbar$ is the Dirac constant, μ is the chemical potential, and $\hat{n}_i = \hat{c}_i^\dagger \hat{c}_i$. The model is defined on the graphite sheet imposing the periodic boundary condition with respect to the chiral vector $\boldsymbol{L}$, which is characterized by the chiral index (n, m) as $\boldsymbol{L} = n\boldsymbol{a}_1 + m\boldsymbol{a}_2$ [see Fig. 1(b)] [73]. The effects of the magnetic and electric fields are included via the Peierls phase through the vector potential $\boldsymbol{A}(t) = \boldsymbol{A}_B + \boldsymbol{A}_E(t)$. The contribution from the static magnetic field is $\boldsymbol{A}_B = A_B \boldsymbol{e}_\perp$ and that from the electric field is $\boldsymbol{A}_E(t) = A_E(t)\boldsymbol{e}_\parallel$. $A_B = \frac{B\cdot|\boldsymbol{L}|}{4\pi}$ and $E(t) = -\partial_t A_E(t)$. $\boldsymbol{e}_\parallel$ and $\boldsymbol{e}_\perp$ are unit vectors of the tube

 ©2023 American Physical Society

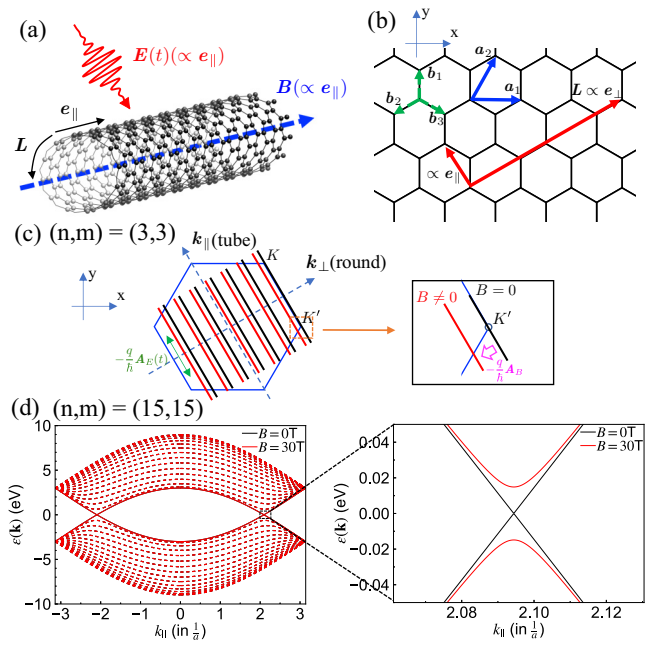

FIG. 1. (a) A CNT with a static magnetic field ($\boldsymbol{B} = B\boldsymbol{e}_\parallel$) and ac electric field ($\boldsymbol{E}(t) = E(t)\boldsymbol{e}_\parallel$) along the tube. (b) A graphite sheet. $\boldsymbol{b}_i$ represents the vector from a site of the A sublattice to neighboring sites of the B sublattice. $\mathbf{a}_1$ and $\mathbf{a}_2$ are primitive translation vectors. $\boldsymbol{L} \equiv n\mathbf{a}_1 + m\mathbf{a}_2$ ($\propto \boldsymbol{e}_\perp$) is the chiral vector characterizing CNTs. $\boldsymbol{e}_\parallel$ and $\boldsymbol{e}_\perp$ are unit vectors of the tube and circumferential directions. (c) Correspondence of the momentum of an armchair CNT and that of graphene. The blue hexagon is the BZ of graphene, where K and K' are the Dirac points. (d) The band structure of the armchair CNT with $(n, m) = (15, 15)$ with and without a static magnetic field. The solid line indicates the bands closest to K and K', which form 1D Dirac systems.

and circumferential directions, respectively [see Fig. 1(b)]. In the following, we focus on the armchair CNT with the chiral index (n, m) with $n = m$.

The Fourier transform of the Hamiltonian (1) is $\hat{H}(t) = \sum_{\boldsymbol{k}} \hat{\boldsymbol{\psi}}_{\boldsymbol{k}}^\dagger \mathbf{h}(\boldsymbol{k}(t))\hat{\boldsymbol{\psi}}_{\boldsymbol{k}}$, where

$$\mathbf{h}(\boldsymbol{k}) = \begin{bmatrix} -\mu & F(\boldsymbol{k}) \\ F^*(\boldsymbol{k}) & -\mu \end{bmatrix}, \tag{2}$$

and $\boldsymbol{k}(t) \equiv \boldsymbol{k} - \frac{q}{\hbar}\boldsymbol{A}(t)$ [see the Supplemental Material (SM) [74] for details]. Here, $\hat{\boldsymbol{\psi}}_{\boldsymbol{k}}^\dagger = [\hat{c}_{\boldsymbol{k}A}^\dagger, \hat{c}_{\boldsymbol{k}B}^\dagger]$, $\hat{c}_{\boldsymbol{k}A}^\dagger$, and $\hat{c}_{\boldsymbol{k}B}^\dagger$ are the Fourier transforms of $\hat{c}_i^\dagger$ on the A and B sublattices, respectively, and $F(\boldsymbol{k}) = -t_{\rm hop}[e^{i\boldsymbol{k}\cdot\boldsymbol{b}_1} + e^{i\boldsymbol{k}\cdot\boldsymbol{b}_2} + e^{i\boldsymbol{k}\cdot\boldsymbol{b}_3}]$ [see Fig. 1(b) for $\boldsymbol{b}_i$]. The Hamiltonian (2) is the same as that of graphene [72], and the set of $\boldsymbol{k}_B (\equiv \boldsymbol{k} - \frac{q}{\hbar}\boldsymbol{A}_B)$ for the CNT corresponds to some lines along $\boldsymbol{k}_\perp$ on the Brillouin zone (BZ) of graphene [see Fig. 1(c)]. Note that $\boldsymbol{k}(t) = \boldsymbol{k}_B - \frac{q}{\hbar}\boldsymbol{A}_E(t)$, which moves along $\boldsymbol{k}_\parallel$ in time. For $B = 0$, $\boldsymbol{k}_B$'s for the CNT pass the Dirac points K and K' of graphene, hence the CNT bands host gapless Dirac bands [see Figs. 1(c) and 1(d)]. Meanwhile, for $B \neq 0$, $\boldsymbol{k}_B$'s are shifted by $-\frac{q}{\hbar}\boldsymbol{A}_B$ and do not pass the Dirac points. Hence the CNT bands host gapful Dirac bands. Around the Dirac points, the Hamiltonian (2) is effectively described by the Dirac model [see Fig. 1(d) and SM [74] for details]. In our setup, the dynamics of electrons around the Dirac points leads to HHG, which is captured by this model.

The diameters of single-wall CNTs are typically 0.7–2 nm [75]. The static magnetic field applied to CNTs in optical experiments can be several tens of tesla [68]. In the following, we set $t_{\rm hop} = 3$ eV and $a = 0.246$ nm and focus on the CNT with $(n, m) = (15, 15)$, whose diameter is 2.04 nm. The band gap for $B = 30$ T becomes 29.7 meV ($\simeq$7.5 THz) [see Fig. 1(d)]. We mainly focus on half filling ($\mu = 0$) and apply the Gaussian electric field described by $A_E(t) = \frac{E_0}{\hbar\Omega}\exp[-\frac{(t-t_0)^2}{2\sigma^2}]\sin[\Omega(t - t_0)]$. We set the electric-field frequency $\hbar\Omega = 10$ meV ($\simeq$2.5 THz), the pulse center $t_0 = 3.95$ ps, and the pulse width $\sigma = 658$ fs, in the main text.

We simulate the time evolution of the tight-binding and Dirac models using the semiconductor Bloch equation (SBE) [76,77]

$$\partial_t \boldsymbol{\rho}_{\boldsymbol{k}}(t) = \frac{i}{\hbar}[\boldsymbol{\rho}_{\boldsymbol{k}}(t), \mathbf{h}(\boldsymbol{k}(t))] - \frac{\boldsymbol{\rho}_{\boldsymbol{k}}(t) - \boldsymbol{\rho}_{{\rm eq},\boldsymbol{k}(t)}}{T_1} + \left(\frac{1}{T_1} - \frac{1}{T_2}\right)\mathbf{U}(\boldsymbol{k}(t))\boldsymbol{\rho}_{{\rm off},\boldsymbol{k}}^{\rm H}(t)\mathbf{U}^\dagger(\boldsymbol{k}(t)), \tag{3}$$

where $\boldsymbol{\rho}_{\boldsymbol{k}}(t)$ is the single-particle density matrix consisting of $\rho_{\alpha\beta,\boldsymbol{k}}(t) = \langle \hat{c}_{\boldsymbol{k}\beta}^\dagger(t)\hat{c}_{\boldsymbol{k}\alpha}(t)\rangle$ with $\alpha, \beta = A, B$. The last two terms express the relaxation processes within the relaxation-time approximation. $\boldsymbol{\rho}_{{\rm eq},\boldsymbol{k}}$ is the equilibrium density matrix for the initial temperature (T). $\mathbf{U}(\boldsymbol{k})$ is a unitary matrix diagonalizing $\mathbf{h}(\boldsymbol{k})$ as $\mathbf{U}^\dagger(\boldsymbol{k})\mathbf{h}(\boldsymbol{k})\mathbf{U}(\boldsymbol{k}) = \boldsymbol{\epsilon}(\boldsymbol{k})$ with $\boldsymbol{\epsilon}(\boldsymbol{k}) = {\rm diag}[\epsilon_0(\boldsymbol{k}), \epsilon_1(\boldsymbol{k})]$. It offers the description in the band (Houston) basis. In this basis, the density matrix becomes $\boldsymbol{\rho}_{\boldsymbol{k}}^{\rm H}(t) \equiv \mathbf{U}^\dagger(\boldsymbol{k}(t))\boldsymbol{\rho}_{\boldsymbol{k}}(t)\mathbf{U}(\boldsymbol{k}(t))$, whose off-diagonal components are $\boldsymbol{\rho}_{{\rm off},\boldsymbol{k}}^{\rm H}(t)$ [72]. The diagonal components of $\boldsymbol{\rho}_{\boldsymbol{k}}^{\rm H}$ indicate the occupation of the bands, and the off-diagonal components indicate the interband hybridization. Thus, T_1 represents the relaxation time of the band occupation, while T_2 represents the dephasing time of the interband coherence. We set $T_1 = 98.8$ fs and $T_2 = 19.8$ fs to be consistent with previous studies for graphene and CNTs [59,78–81].

The light radiation originates from the oscillation of electric polarization (or corresponding current) [82]. Since the current along the circumferential direction does not yield polarization, the HHG spectrum (normalized by the number of sites) is evaluated from $J_\parallel(t)$ (the current along $\boldsymbol{e}_\parallel$) as $I_{\rm HHG}(\omega) = |\omega J_\parallel(\omega)|^2$. Here, $J_\parallel(\omega) = \int dt e^{i\omega t} J_\parallel(t)$, and $J_\parallel(t)$ is evaluated from $\rho_{\alpha\beta,\boldsymbol{k}}(t)$ using the current operator $\hat{J}_\parallel(t) \equiv -\frac{1}{N}\frac{\delta\hat{H}(t)}{\delta A_E(t)}$. $2N$ is the number of atoms (sites) for the CNT. In the conditions studied here, HHG mainly originates from the bands closest to the Dirac points, i.e., solid lines in Fig. 1(d).

Figure 2(a) shows $I_{\rm HHG}$ of the armchair CNT with and without the magnetic field obtained from the tight-binding model. Only odd harmonics components appear in $I_{\rm HHG}(\omega)$, because the system (1) is symmetric under a time-space operation, $t \to t + \frac{\pi}{\Omega}$ and $\mathbf{e}_\parallel \to -\mathbf{e}_\parallel$ during the time-periodic excitation (see Ref. [83] for a general argument). When $B = 0$ the intensity for $l(\geqslant 3)$th harmonics is very small. When $B \neq 0$ the HHG intensity for $l \geqslant 3$ is strongly enhanced by more than several orders of magnitude. Figure 2(b) shows the intensity at the HHG peaks $I_{\rm peak}(l)$ as a function of B for $l = 3, 5, 7$. $I_{\rm peak}(l)$ is defined as the maximum value of

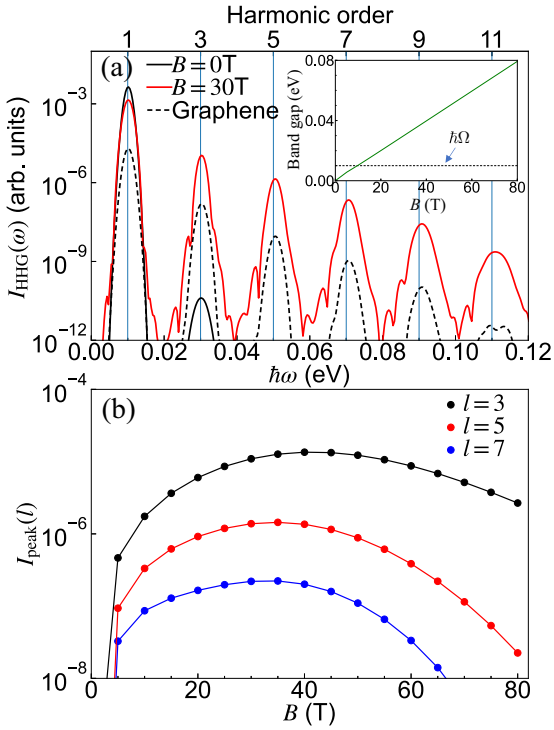

FIG. 2. (a) HHG spectra $I_{\rm HHG}$ of the armchair CNT with and without the static magnetic field simulated with the tight-binding model. $I_{\rm HHG}$ for graphene is also shown. The inset show the band gap induced by the magnetic field B. (b) The intensity at the HHG peaks $I_{\rm peak}(l)$ as a function of B. We set the chiral index $(n, m) = (15, 15)$, $\mu = 0$, $T = 11.6$ K, $T_1 = 98.8$ fs, and $T_2 = 19.8$ fs. The parameters of the electric field are $\hbar\Omega = 10$ meV and $E_0 = 30$ kV/cm.

$I_{\rm HHG}(\omega)$ for $\omega \in [l\Omega - \Omega, l\Omega + \Omega]$. $I_{\rm peak}(l)$ is nonmonotonic against B, since a gap too large compared to Ω suppresses the excitation and thus HHG [see the inset of Fig. 2(a)]. Namely, there exists the optimal value of B maximizing $I_{\rm HHG}(\omega)$ for a given E_0. Furthermore, the HHG intensity in the CNT per atom for this optimal B is much larger than that in graphene per atom [see Fig. 2(a)]. This is understood as follows. In the CNT, we can tune B such that the bands closest to the Dirac points yield HHG most efficiently for a given E_0, and the contributions from the rest of the bands are negligible. Meanwhile, in graphene, which is identical to a CNT with $n, m \to \infty$, the number of bands along $\boldsymbol{k}_\parallel$ contributing to HHG increases. However, the contribution from each band is not optimal for a given electric-field condition, and they may interfere and cancel each other on average. We also note that the drastic enhancement of HHG with B can be observed even for doped CNTs or for higher-frequency excitations (see SM [74]).

The efficiency of the enhancement depends on the chiral index $n(= m)$. First, the momentum shift due to the AB effect is $\frac{q}{\hbar}A_B$, which is proportional to B and $L(\equiv |\boldsymbol{L}| \propto n)$. Therefore, in order to realize a given value of A_B (or the gap), smaller B is required for larger n (see SM [74] for examples). Thus, as far as only the bands closest to the Dirac points are involved in HHG, a larger n is favorable for the efficient control of HHG. Meanwhile, with increasing n, the number of bands along $\boldsymbol{k}_\parallel$ increases, and many bands start to contribute to HHG. Then, the impact of the AB effect on HHG becomes less prominent. In the extreme limit of $n \to \infty$ (graphene), the AB effect has no impact on physical properties.

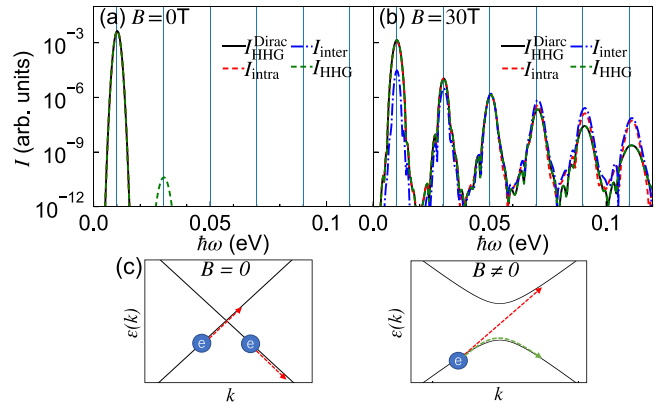

FIG. 3. (a), (b) Comparison of the HHG spectra of the armchair CNT obtained in different ways for (a) $B = 0$ T and (b) $B = 30$ T. $I_{\rm HHG}(\omega)$ is evaluated from the tight-binding model, while $I_{\rm HHG}^{\rm Dirac}(\omega)$, $I_{\rm intra}(\omega)$, and $I_{\rm inter}(\omega)$ are evaluated from the Dirac model considering only bands closest to K or K'. The parameters of the system and the electric field are the same as Fig. 2. (c) The dynamics of electrons with and without the magnetic field. The momentum shift originates from the intraband acceleration by the electric field.

To understand the origin of the enhancement of HHG with the magnetic field, we compare the HHG intensity evaluated from the tight-binding model ($I_{\rm HHG}$) and that from the Dirac model ($I_{\rm HHG}^{\rm Dirac}$) [see Figs. 3(a) and 3(b)]. We only consider the contributions from the bands closest to K and K' for the Dirac model. The results from the Dirac model match well those from the tight-binding model both for $B = 0$ and $B = 30$ T. The only exception is the third harmonic generation at $B = 0$, which originates from the nonlinear part of the band dispersion. Namely, the 1D gapless Dirac model shows no HHG at $B = 0$. Simply speaking, this is because the transition of electrons between bands in the 1D gapless Dirac system under an electric field is always perfect and electrons never change the velocity [see Fig. 3(c)]. Without the relaxation, this leads to $J_\parallel(t) \propto A_E(t)$ [84,85]. If we take into account the relaxation, we obtain

$$\partial_t J_\parallel(t) = \frac{1}{n}\frac{t_{\rm hop}}{\hbar}\sigma_0 E(t) - \frac{1}{T_1}J_\parallel(t), \tag{4}$$

from the SBE (3), where $\sigma_0 = \frac{\sqrt{3}a^2q^2}{2\pi\hbar}$ (see SM [74]). This is a linear differential equation, leading to no HHG. The last term of Eq. (4), which we call $[\partial_t J_\parallel(t)]_{\rm corr}$, originates from the relaxation term of the SBE. The present form originates from the relaxation-time approximation in Eq. (3). In principle, if $[\partial_t J_\parallel(t)]_{\rm corr}$ depends on $J_\parallel$ nonlinearly, the 1D gapless Dirac system can show HHG. Still, in a previous experiment of HHG in CNTs [64], metallic CNTs show very weak HHG, which is consistent with the consequence from Eq. (4).

To obtain further insight, we evaluate the contribution from the intraband current ($I_{\rm intra} = |\omega J_{\parallel,{\rm intra}}(\omega)|^2$) and that from the interband current ($I_{\rm inter} = |\omega J_{\parallel,{\rm inter}}(\omega)|^2$) using the Dirac model. We define the intraband current as $J_{\parallel,{\rm intra}}(t) \equiv \frac{q}{\hbar N}\sum_{\boldsymbol{k}} {\rm Tr}[\boldsymbol{\rho}_{\boldsymbol{k}}^H(t)\partial_{k_\parallel}\boldsymbol{\epsilon}(\boldsymbol{k}(t))]$ and the interband

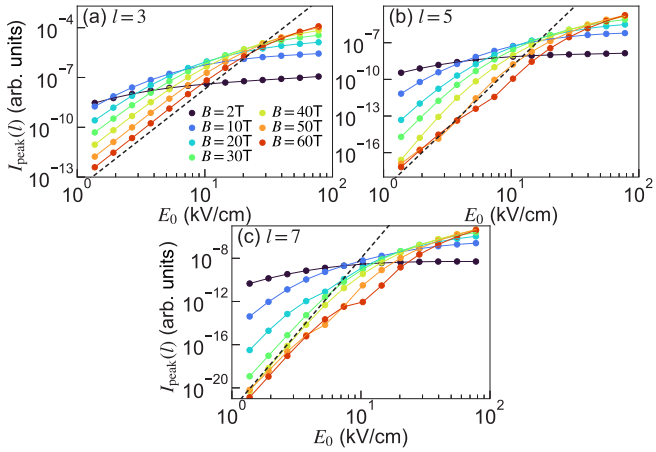

FIG. 4. The intensity at the HHG peaks $I_{\rm peak}(l)$ for the armchair CNT as a function of the strength of the ac electric field E_0 for (a) $l = 3$, (b) $l = 5$, and (c) $l = 7$. The tight-binding model is used. The dashed lines are proportional to $(E_0)^{2l}$ for each panel. The parameters of the system and the electric field are the same as in Fig. 2.

current as $J_{\parallel,\rm inter}(t) \equiv J_\parallel(t) - J_{\parallel,\rm intra}(t)$. The former is associated with the change in the band occupation, while the latter is associated with that of the interband polarization [the off-diagonal component of $\boldsymbol{\rho}_{\boldsymbol{k}}^H(t)$] (see SM [74] for details). When $B = 0$, the perfect transition between the conduction and valence bands happens without inducing the interband polarization, leading to $I_{\rm HHG} = I_{\rm intra}$ [see Fig. 3(c)]. Meanwhile, when $B \neq 0$, the gap opens and the dipole moments between the bands become finite. These allow electrons to stay in the same band and tunnel to the other band changing their group velocity [see Fig. 3(c)]. Thus, both the intraband and interband currents are activated to contribute to HHG [see Fig. 3(b)]. In the present case, the gap and the excitation frequency are comparable, which makes the contributions from these currents comparable. The HHG contributions from $J_{\parallel,\rm intra}(t)$ and $J_{\parallel,\rm inter}(t)$ cancel each other due to their interference.

Finally, we discuss the dependence on the strength of the applied ac electric field E_0 [see Fig. 1(a)]. In Fig. 4, we show the intensity at the HHG peaks $I_{\rm peak}(l)$ as a function of E_0 for $l = 3, 5, 7$. In the perturbative regime with respect to E_0, we expect $I_{\rm peak}(l) \propto (E_0)^{2l}$. (For small B, this perturbative behavior is recovered with E_0 below the range shown in Fig. 4.) For all harmonics, the deviation from the perturbative regime happens at larger E_0 for larger B, i.e., larger gap. $I_{\rm peak}(l)$ tends to be saturated due to the higher-order corrections. Because of this, the value of B maximizing $I_{\rm peak}(l)$ for a given E_0 depends on the value of E_0. Namely, when E_0 is small, the optimal B is small, while for larger E_0, the optimal B becomes large. We note that these properties are insensitive to the choice of T_1 and T_2 (see SM [74]).

One interesting observation is that the optimal value of B continuously decreases with decreasing E_0 and it becomes a few tesla for $E_0 \sim 1$ kV/cm. This indicates that $\sigma^{(l)}$ monotonically increases with decreasing B. Here, $\sigma^{(l)}$ represents the lth-order optical conductivity, i.e., $J_\parallel(l\Omega) \simeq \sigma^{(l)}(E_0)^l$. However, this peculiar behavior turns out to be sensitive to the choice of T_1 and T_2 (see SM [74]). When $T_1 = T_2$, the optimal B for small E_0 remains around 20 T, where the gap is almost double of Ω. The crucial dependence on T_1 and T_2 can be attributed to the change in cancellation between the interband and intraband currents. This point can be directly seen in the analytic expression of $\sigma^{(3)}$. If we express contributions from $J_{\rm inter}$ and $J_{\rm intra}$ as $\sigma^{(3)}_{\rm inter}$ and $\sigma^{(3)}_{\rm intra}$, the leading terms in the limit of $B \to 0$ read

$$\sigma^{(3)}_{\rm intra} \simeq -F\frac{1}{A_B^2}\frac{1}{\zeta_3}, \quad \sigma^{(3)}_{\rm inter} \simeq F\frac{1}{A_B^2}\frac{1}{\xi_3},$$
$$F \equiv i\sigma_0 t_{\rm hop}\hbar^2\frac{1}{n}\frac{1}{\xi_1}\left(\frac{\lambda_0}{2\zeta_2} + \frac{\lambda_2}{\xi_2}\right), \tag{5}$$

at $T = 0$. Here, $\zeta_m = m\hbar\Omega + i\hbar/T_1$, $\xi_m = m\hbar\Omega + i\hbar/T_2$, and $\lambda_m = \int dx \frac{x^m}{\sqrt{1+x^2}}$. The expression tells that $\sigma^{(3)}$ diverges for $B \to 0$ when $T_1 \neq T_2$, while the divergence is absent when $T_1 = T_2$ due to the cancellation between $\sigma^{(3)}_{\rm inter}$ and $\sigma^{(3)}_{\rm intra}$. Our numerical simulation suggests that the same happens also for higher harmonics with $l \geqslant 5$. Namely, for $T_1 = T_2$, the contributions from the interband and intraband currents cancel each other efficiently, while for $T_1 \neq T_2$, the cancellation becomes weaker (see SM [74]). Although we used $T_1 = 98.8$ fs and $T_2 = 19.8$ fs to be consistent with previous studies, to fully determine the realistic choice of T_1 and T_2 for the present energy scale, a microscopic evaluation of the relaxation and dephasing processes is required [86–91].

To summarize, we showed that HHG in metallic CNTs can be drastically manipulated in the THz regime using the AB effect. Tuning the strength of the magnetic field, the HHG intensity can be maximized, where HHG per atom is more efficient than in graphene. Such controllability of HHG may be useful to develop an efficient HHG device in the THz regime. In addition, with realistic parameters of CNTs and external fields, a metallic CNT under magnetic fields can be regarded as a tunable 1D Dirac system for THz excitations. Therefore, it serves as a useful platform to systematically study HHG in Dirac systems. Furthermore, the unique idea of manipulating HHG via the AB effect can be applied for all kinds of nanotubes including semiconducting CNTs, boron nitride nanotubes [92,93], and transition-metal dichalcogenide nanotubes [94].

We would like to acknowledge fruitful discussions with Hiroyuki Nishidome and Kazuhiro Yanagi. This work is supported by Grant-in-Aid for Scientific Research from JSPS, KAKENHI Grants No. JP20K14412, No. JP21H05017 (Y.M.), No. JP22K03525, No. JP21H01025, No. JP19H05821 (A.K.), and JST CREST Grant No. JPMJCR1901 (Y.M.).

[1] S. Y. Kruchinin, F. Krausz, and V. S. Yakovlev, Rev. Mod. Phys. **90**, 021002 (2018).

[2] C. Giannetti, M. Capone, D. Fausti, M. Fabrizio, F. Parmigiani, and D. Mihailovic, Adv. Phys. **65**, 58 (2016).

[3] D. N. Basov, R. D. Averitt, and D. Hsieh, Nat. Mater. **16**, 1077 (2017).
[4] A. Cavalleri, Contemp. Phys. **59**, 31 (2018).
[5] T. Oka and S. Kitamura, Annu. Rev. Condens. Matter Phys. **10**, 387 (2019).
[6] A. de la Torre, D. M. Kennes, M. Claassen, S. Gerber, J. W. McIver, and M. A. Sentef, Rev. Mod. Phys. **93**, 041002 (2021).
[7] S. Koshihara, T. Ishikawa, Y. Okimoto, K. Onda, R. Fukaya, M. Hada, Y. Hayashi, S. Ishihara, and T. Luty, Phys. Rep. **942**, 1 (2022).
[8] P. B. Corkum and F. Krausz, Nat. Phys. **3**, 381 (2007).
[9] F. Krausz and M. Ivanov, Rev. Mod. Phys. **81**, 163 (2009).
[10] S. Ghimire and D. A. Reis, Nat. Phys. **15**, 10 (2019).
[11] M. Ferray, A. L'Huillier, X. F. Li, L. A. Lompre, G. Mainfray, and C. Manus, J. Phys. B: At., Mol. Opt. Phys. **21**, L31 (1988).
[12] P. B. Corkum, Phys. Rev. Lett. **71**, 1994 (1993).
[13] M. Lewenstein, P. Balcou, M. Y. Ivanov, A. L'Huillier, and P. B. Corkum, Phys. Rev. A **49**, 2117 (1994).
[14] S. Ghimire, A. D. DiChiara, E. Sistrunk, P. Agostini, L. F. DiMauro, and D. A. Reis, Nat. Phys. **7**, 138 (2011).
[15] O. Schubert, M. Hohenleutner, F. Langer, B. Urbanek, C. Lange, U. Huttner, D. Golde, T. Meier, M. Kira, S. W. Koch, and R. Huber, Nat. Photonics **8**, 119 (2014).
[16] G. Vampa, C. R. McDonald, G. Orlando, D. D. Klug, P. B. Corkum, and T. Brabec, Phys. Rev. Lett. **113**, 073901 (2014).
[17] T. T. Luu, M. Garg, S. Y. Kruchinin, A. Moulet, M. T. Hassan, and E. Goulielmakis, Nature (London) **521**, 498 (2015).
[18] G. Vampa, T. J. Hammond, N. Thire, B. E. Schmidt, F. Legare, C. R. McDonald, T. Brabec, and P. B. Corkum, Nature (London) **522**, 462 (2015).
[19] F. Langer, M. Hohenleutner, C. P. Schmid, C. Pöllmann, P. Nagler, T. Korn, C. Schüller, M. Sherwin, U. Huttner, J. Steiner, S. Koch, M. Kira, and R. Huber, Nature (London) **533**, 225 (2016).
[20] M. Hohenleutner, F. Langer, O. Schubert, M. Knorr, U. Huttner, S. Koch, M. Kira, and R. Huber, Nature (London) **523**, 572 (2015).
[21] G. Ndabashimiye, S. Ghimire, M. Wu, D. A. Browne, K. J. Schafer, M. B. Gaarde, and D. A. Reis, Nature (London) **534**, 520 (2016).
[22] T. Otobe, Phys. Rev. B **94**, 235152 (2016).
[23] N. Tancogne-Dejean, O. D. Mücke, F. X. Kärtner, and A. Rubio, Nat. Commun. **8**, 745 (2017).
[24] T. Ikemachi, Y. Shinohara, T. Sato, J. Yumoto, M. Kuwata-Gonokami, and K. L. Ishikawa, Phys. Rev. A **95**, 043416 (2017).
[25] H. Liu, Y. Li, Y. S. You, S. Ghimire, T. F. Heinz, and D. A. Reis, Nat. Phys. **13**, 262 (2017).
[26] Y. S. You, D. Reis, and S. Ghimire, Nat. Phys. **13**, 345 (2017).
[27] K. Kaneshima, Y. Shinohara, K. Takeuchi, N. Ishii, K. Imasaka, T. Kaji, S. Ashihara, K. L. Ishikawa, and J. Itatani, Phys. Rev. Lett. **120**, 243903 (2018).
[28] F. Sekiguchi, G. Yumoto, H. Hirori, and Y. Kanemitsu, Phys. Rev. B **106**, L241201 (2022).
[29] F. Giorgianni, E. Chiadroni, A. Rovere, M. Cestelli-Guidi, A. Perucchi, M. Bellaveglia, M. Castellano, D. Di Giovenale, G. Di Pirro, M. Ferrario, R. Pompili, C. Vaccarezza, F. Villa, A. Cianchi, A. Mostacci, M. Petrarca, M. Brahlek, N. Koirala, S. Oh, and S. Lupi, Nat. Commun. **7**, 11421 (2016).
[30] N. Yoshikawa, T. Tamaya, and K. Tanaka, Science **356**, 736 (2017).
[31] H. A. Hafez, S. Kovalev, J.-C. Deinert, Z. Mics, B. Green, N. Awari, M. Chen, S. Germanskiy, U. Lehnert, J. Teichert, Z. Wang, K.-J. Tielrooij, Z. Liu, Z. Chen, A. Narita, K. Mullen, M. Bonn, M. Gensch, and D. Turchinovich, Nature (London) **561**, 507 (2018).
[32] R. E. F. Silva, Á. Jiménez-Galán, B. Amorim, O. Smirnova, and M. Ivanov, Nat. Photonics **13**, 849 (2019).
[33] A. Chacón, D. Kim, W. Zhu, S. P. Kelly, A. Dauphin, E. Pisanty, A. S. Maxwell, A. Picón, M. F. Ciappina, D. E. Kim, C. Ticknor, A. Saxena, and M. Lewenstein, Phys. Rev. B **102**, 134115 (2020).
[34] B. Cheng, N. Kanda, T. N. Ikeda, T. Matsuda, P. Xia, T. Schumann, S. Stemmer, J. Itatani, N. P. Armitage, and R. Matsunaga, Phys. Rev. Lett. **124**, 117402 (2020).
[35] C. P. Schmid, L. Weigl, P. Grössing, V. Junk, C. Gorini, S. Schlauderer, S. Ito, M. Meierhofer, N. Hofmann, D. Afanasiev, J. Crewse, K. A. Kokh, O. E. Tereshchenko, J. Güdde, F. Evers, J. Wilhelm, K. Richter, U. Höfer, and R. Huber, Nature (London) **593**, 385 (2021).
[36] D. Baykusheva, A. Chacón, J. Lu, T. P. Bailey, J. A. Sobota, H. Soifer, P. S. Kirchmann, C. Rotundu, C. Uher, T. F. Heinz, D. A. Reis, and S. Ghimire, Nano Lett. **21**, 8970 (2021).
[37] R. E. F. Silva, I. V. Blinov, A. N. Rubtsov, O. Smirnova, and M. Ivanov, Nat. Photon. **12**, 266 (2018).
[38] Y. Murakami, M. Eckstein, and P. Werner, Phys. Rev. Lett. **121**, 057405 (2018).
[39] N. Tancogne-Dejean, M. A. Sentef, and A. Rubio, Phys. Rev. Lett. **121**, 097402 (2018).
[40] S. Imai, A. Ono, and S. Ishihara, Phys. Rev. Lett. **124**, 157404 (2020).
[41] Y. Murakami, S. Takayoshi, A. Koga, and P. Werner, Phys. Rev. B **103**, 035110 (2021).
[42] C. Orthodoxou, A. Zaïr, and G. H. Booth, npj Quantum Mater. **6**, 76 (2021).
[43] M. Udono, K. Sugimoto, T. Kaneko, and Y. Ohta, Phys. Rev. B **105**, L241108 (2022).
[44] M. R. Bionta, E. Haddad, A. Leblanc, V. Gruson, P. Lassonde, H. Ibrahim, J. Chaillou, N. Émond, M. R. Otto, A. Jiménez-Galán, R. E. F. Silva, M. Ivanov, B. J. Siwick, M. Chaker, and F. Légaré, Phys. Rev. Res. **3**, 023250 (2021).
[45] C. Shao, H. Lu, X. Zhang, C. Yu, T. Tohyama, and R. Lu, Phys. Rev. Lett. **128**, 047401 (2022).
[46] T. Hansen, S. Vendelbo Bylling Jensen, and L. B. Madsen, Phys. Rev. A **105**, 053118 (2022).
[47] K. Uchida, G. Mattoni, S. Yonezawa, F. Nakamura, Y. Maeno, and K. Tanaka, Phys. Rev. Lett. **128**, 127401 (2022).
[48] Y. Murakami, K. Uchida, A. Koga, K. Tanaka, and P. Werner, Phys. Rev. Lett. **129**, 157401 (2022).
[49] T. Hansen and L. B. Madsen, Phys. Rev. B **106**, 235142 (2022).
[50] O. Grånäs, I. Vaskivskyi, X. Wang, P. Thunström, S. Ghimire, R. Knut, J. Söderström, L. Kjellsson, D. Turenne, R. Y. Engel, M. Beye, J. Lu, D. J. Higley, A. H. Reid, W. Schlotter, G. Coslovich, M. Hoffmann, G. Kolesov, C. Schüßler-Langeheine, A. Styervoyedov *et al.*, Phys. Rev. Res. **4**, L032030 (2022).
[51] G. Y. Slepyan, S. A. Maksimenko, V. P. Kalosha, J. Herrmann, E. E. B. Campbell, and I. V. Hertel, Phys. Rev. A **60**, R777 (1999).
[52] S. A. Mikhailov, Europhys. Lett. **79**, 27002 (2007).

[53] A. R. Wright, X. G. Xu, J. C. Cao, and C. Zhang, Appl. Phys. Lett. **95**, 072101 (2009).
[54] I. Al-Naib, J. E. Sipe, and M. M. Dignam, Phys. Rev. B **90**, 245423 (2014).
[55] I. Al-Naib, M. Poschmann, and M. M. Dignam, Phys. Rev. B **91**, 205407 (2015).
[56] J. L. Cheng, N. Vermeulen, and J. E. Sipe, Phys. Rev. B **91**, 235320 (2015).
[57] L. A. Chizhova, F. Libisch, and J. Burgdörfer, Phys. Rev. B **95**, 085436 (2017).
[58] M. S. Mrudul and G. Dixit, Phys. Rev. B **103**, 094308 (2021).
[59] S. A. Sato, H. Hirori, Y. Sanari, Y. Kanemitsu, and A. Rubio, Phys. Rev. B **103**, L041408 (2021).
[60] D. Baykusheva, A. Chacón, D. Kim, D. E. Kim, D. A. Reis, and S. Ghimire, Phys. Rev. A **103**, 023101 (2021).
[61] S. Kovalev, R. M. A. Dantas, S. Germanskiy, J.-C. Deinert, B. Green, I. Ilyakov, N. Awari, M. Chen, M. Bawatna, J. Ling, F. Xiu, P. H. M. van Loosdrecht, P. Surówka, T. Oka, and Z. Wang, Nat. Commun. **11**, 2451 (2020).
[62] M. J. Paul, Y. C. Chang, Z. J. Thompson, A. Stickel, J. Wardini, H. Choi, E. D. Minot, B. Hou, J. A. Nees, T. B. Norris, and Y.-S. Lee, New J. Phys. **15**, 085019 (2013).
[63] T. Tamaya and T. Kato, Phys. Rev. B **103**, 205202 (2021).
[64] H. Nishidome, K. Nagai, K. Uchida, Y. Ichinose, Y. Yomogida, Y. Miyata, K. Tanaka, and K. Yanagi, Nano Lett. **20**, 6215 (2020).
[65] S. de Vega, J. D. Cox, F. Sols, and F. J. García de Abajo, Phys. Rev. Res. **2**, 013313 (2020).
[66] H. Ajiki and T. Ando, J. Phys. Soc. Jpn. **62**, 1255 (1993).
[67] H. Ajiki and T. Ando, Phys. B: Condens. Matter **201**, 349 (1994).
[68] S. Zaric, G. N. Ostojic, J. Kono, J. Shaver, V. C. Moore, M. S. Strano, R. H. Hauge, R. E. Smalley, and X. Wei, Science **304**, 1129 (2004).
[69] R. Matsunaga, K. Matsuda, and Y. Kanemitsu, Phys. Rev. Lett. **101**, 147404 (2008).
[70] J. Li, D. Golez, G. Mazza, A. J. Millis, A. Georges, and M. Eckstein, Phys. Rev. B **101**, 205140 (2020).
[71] M. Schüler, J. A. Marks, Y. Murakami, C. Jia, and T. P. Devereaux, Phys. Rev. B **103**, 155409 (2021).
[72] Y. Murakami and M. Schüler, Phys. Rev. B **106**, 035204 (2022).
[73] N. Hamada, S.-I. Sawada, and A. Oshiyama, Phys. Rev. Lett. **68**, 1579 (1992).
[74] See Supplemental Material at http://link.aps.org/supplemental/10.1103/PhysRevB.108.L241202 for the details of the model and numerical method; the derivation of Eqs. (4) and (5); the doping effects; the dependence of the excitation frequency; the dependence on the chiral index; and the effects of the relaxation times, which includes Refs. [95–98].
[75] K. Yanagi, Y. Miyata, and H. Kataura, Appl. Phys. Express **1**, 034003 (2008).
[76] U. Huttner, M. Kira, and S. W. Koch, Laser Photonics Rev. **11**, 1700049 (2017).
[77] L. Yue and M. B. Gaarde, J. Opt. Soc. Am. B **39**, 535 (2022).
[78] B. F. Habenicht, H. Kamisaka, K. Yamashita, and O. V. Prezhdo, Nano Lett. **7**, 3260 (2007).
[79] P. A. George, J. Strait, J. Dawlaty, S. Shivaraman, M. Chandrashekhar, F. Rana, and M. G. Spencer, Nano Lett. **8**, 4248 (2008).
[80] S. Tani, F. Blanchard, and K. Tanaka, Phys. Rev. Lett. **109**, 166603 (2012).
[81] C. Heide, T. Eckstein, T. Boolakee, C. Gerner, H. B. Weber, I. Franco, and P. Hommelhoff, Nano Lett. **21**, 9403 (2021).
[82] J. D. Jackson, *Classical Electrodynamics* (Wiley, New York, 1998).
[83] O. Neufeld, D. Podolsky, and O. Cohen, Nat. Commun. **10**, 405 (2019).
[84] K. L. Ishikawa, Phys. Rev. B **82**, 201402(R) (2010).
[85] Ó. Zurrón-Cifuentes, R. Boyero-García, C. Hernández-García, and L. Plaja, Opt. Express **28**, 19760 (2020).
[86] E. Malic, T. Winzer, E. Bobkin, and A. Knorr, Phys. Rev. B **84**, 205406 (2011).
[87] A. F. Kemper, B. Moritz, J. K. Freericks, and T. P. Devereaux, New J. Phys. **15**, 023003 (2013).
[88] G. Stefanucci and R. v. Leeuwen, *Nonequilibrium Many-Body Theory of Quantum Systems: A Modern Introduction* (Cambridge University Press, Cambridge, UK, 2013).
[89] M. Schüler, D. Golež, Y. Murakami, N. Bittner, A. Herrmann, H. U. Strand, P. Werner, and M. Eckstein, Comput. Phys. Commun. **257**, 107484 (2020).
[90] M. Ridley, N. W. Talarico, D. Karlsson, N. L. Gullo, and R. Tuovinen, J. Phys. A: Math. Theor. **55**, 273001 (2022).
[91] H. Rostami and E. Cappelluti, Phys. Rev. B **103**, 125415 (2021).
[92] A. Rubio, J. L. Corkill, and M. L. Cohen, Phys. Rev. B **49**, 5081 (1994).
[93] N. G. Chopra, R. J. Luyken, K. Cherrey, V. H. Crespi, M. L. Cohen, S. G. Louie, and A. Zettl, Science **269**, 966 (1995).
[94] R. Tenne, L. Margulis, M. Genut, and G. Hodes, Nature (London) **360**, 444 (1992).
[95] H. Khosravi, N. Daneshfar, and A. Bahari, Opt. Lett. **34**, 1723 (2009).
[96] D. Dimitrovski, L. B. Madsen, and T. G. Pedersen, Phys. Rev. B **95**, 035405 (2017).
[97] Y. V. Dvuzhilova, I. S. Dvuzhilov, N. N. Konobeeva, and M. B. Belonenko, Int. J. Mod. Phys. B **35**, 2150017 (2021).
[98] J. Wilhelm, P. Grössing, A. Seith, J. Crewse, M. Nitsch, L. Weigl, C. Schmid, and F. Evers, Phys. Rev. B **103**, 125419 (2021).